Deep neural network for lithium isotope fractionation by diffusion in silicate melts Haiyang Luo^{1,*}, Bijaya B. Karki^{1,2,3}, Dipta B. Ghosh², Huiming Bao¹ Department of Geology & Geophysics, Louisiana State University, Baton Rouge, LA 70803, USA Consumer of Geology & Geophysics, Louisiana State University, Baton Rouge, LA 70803, USA Consumer of Geology & Geophysics, Louisiana State University Consumer of Geology & Geoph

7

8

9

10

11

12

13

14

15

16

17

18

19

20

21

22

23

24

25

26

ABSTRACT

Diffusive isotope fractionation has been widely used to explain lithium (Li) isotope variations in minerals and rocks. Isotope mass dependence of Li diffusion can be empirically expressed as $\frac{D_{7Li}}{D_{6Li}} = \left(\frac{6}{7}\right)^{\beta}$, where D is the diffusivity of a Li isotope. The knowledge about temperature and compositional dependence of the β factor which is essential for understanding diffusion profiles and mechanisms still remains unclear. Based on the potential energy and interatomic forces generated by a deep neural network trained with ab initio data, we performed deep potential molecular dynamics (DPMD) simulations of several Li pseudoisotopes (with mass=2, 7, 21, 42 g/mol) in albite, hydrous albite, and model basalt melts to evaluate the β factor. We found that β in albite melt decreases from 0.267 \pm 0.006 at 4000 K to 0.225 \pm 0.004 at 1800 K. The presence of water appears to slightly weaken the temperature dependence of β , with β decreasing from 0.250 ± 0.012 to 0.228 ± 0.031 in hydrous albite melt. The calculated β in model basalt melt takes much smaller values, decreasing from 0.215 ± 0.006 to 0.132 ± 0.015 . Our prediction of β in albite and hydrous albite melts is in good agreement with experimental results. More importantly, our results suggest that Li isotope diffusion in silicate melts is strongly dependent on melt composition. The temperature and compositional effects on β can be explained in terms of ionic porosity and the coupled relationship between Li diffusion and the mobility of the silicate melt network. Based on our results, it is important that the compositional dependence of diffusive Li isotope fractionation is considered when interpreting isotopic variations of Li. This study shows that DPMD is a promising tool to simulate the diffusion of elements and isotopes in silicate melts.

Keywords: Deep neural network; Diffusion; Lithium isotope fractionation; Silicate melts

1. INTRODUCTION

Lithium has two stable isotopes, ⁷Li (92.4%) and ⁶Li (7.6%). A wide range of equilibrium and kinetic Li isotope fractionation has been reported among Earth materials because of the large mass difference (~17%) between ⁷Li and ⁶Li. As such, Li isotope composition has become a powerful geochemical tool for studying continental weathering, crust-mantle recycling, and magmatic processes (Penniston-Dorland et al., 2017; Tomascak et al., 2016). At magmatic temperatures, equilibrium Li isotope fractionation is expected to be minimal (Bigeleisen and Mayer, 1947; Tomascak et al., 1999; Urey, 1947). By contrast, diffusive Li isotope fractionation in minerals and melts is experimentally known to be significant, with ⁶Li diffusing faster than ⁷Li (Dohmen et al., 2010; Richter et al., 2017; Richter et al., 2014; Richter et al., 2003). Lithium as an element diffuses much faster than other elements in minerals and melts because of Li's +1-valence state and small ionic radius. Diffusion profiles of Li and its isotopes have been applied to investigate late-stage, short-lived magmatic processes, including magma recharge, mixing, ascent, cooling, and degassing (Cabato et al., 2013; Charlier et al., 2012; Coogan et al., 2005; Costa et al., 2020; Ellis et al., 2018; Jeffcoate et al., 2007; Lundstrom et al., 2005; Marschall. and Tang., 2020; Neukampf et al., 2019; Parkinson et al., 2007; Vlastelic et al., 2011).

44 Isotopic mass dependence of Li diffusion can be empirically expressed as (Richter et al., 1999):

45
$$\frac{D_{7_{Li}}}{D_{6_{Li}}} = \left(\frac{6}{7}\right)^{\beta},$$
 (1)

where D is the diffusivity or diffusion coefficient of a Li isotope and β is a dimensionless parameter. The β value and its variations with temperature, pressure, and composition characterize the diffusive behavior of Li isotopes. Li isotope fractionation by diffusion in silicate melts is the key factor in determining the accuracy of timescale information extracted from melt inclusions or embayments using Li geospeedometry

or geochronometer. Despite a growing number of studies applying Li geospeedometry to investigate shortlived magmatic processes, there have been only two experimental calibrations of β for Li isotopes in silicate melts (Holycross et al., 2018; Richter et al., 2003). Richter et al. (2003) obtained a β value of 0.215 in a dry basalt-rhyolite diffusion couple experiments at 1350 °C. The type of diffusion experiments performed by Richter et al. (2003) is chemical diffusion, starting with basalt and rhyolite melts that bear distinctly different major elemental compositions. An important assumption made to fit the observed Li isotopes diffusion profile in the chemical diffusion experiment is that the relative difference in the diffusivities of Li isotopes does not change across the diffusion couple, although the diffusivity of Li shows a strong compositional dependence. Compositional dependence of β for Mg and Ca isotopes have been reported by Watkins et al. (2011) in albite-anorthite and albite-diopside melts diffusion couple experiments. It is logical to speculate that β for Li isotopes might also be composition dependent. Holycross et al. (2018) reported a β value of 0.228 for diffusive fractionation of Li isotopes in rhyolite melts containing ~6 wt. % H₂O at 1063-1148 K, and concluded that there is weak or no temperature and compositional dependences of β for Li isotopes in silicate melts after considering the similar β values between theirs and Richter et al.'s (2003). Note that both temperature and composition are different in the two sets of experiments. Therefore, it is likely Holycross et al. (2018) omitted one likely scenario that β for Li isotopes is both temperature and composition dependent, but the two dependences play opposites roles and lead to an apparent insensitivity to the combined effect of temperature and composition.

50

51

52

53

54

55

56

57

58

59

60

61

62

63

64

65

66

67

68

69

70

71

72

73

74

Temperature dependence of β has been recently predicted by first-principles molecular dynamics simulations of Mg isotopes in MgSiO₃ and Mg₂SiO₄ melts (Luo et al., 2020). This relationship has not been resolved in experiments probably due to narrow temperature range (~1623-1773 K) explored. In addition, the diffusion experiments done by Holycross et al. (2018) used juxtaposed hydrous rhyolite glasses in which Li content is the only difference between the two glasses. By contrast, Li diffusion in basalt-rhyolite diffusion couple experiments conducted by Richter et al. (2003) is multicomponent diffusion. The direct comparison between the two β values would make sense only if we assume that β is composition

independent. In brief, the β values of Li in silicate melts over relevant pressure-temperature-composition space are important to high-temperature geological problems but remain poorly constrained.

First-principles molecular dynamics (FPMD) simulations have provided valuable insights into the diffusive behavior of elements in silicate melts (Ghosh and Karki, 2011, 2017; Karki, 2010). Isotope fractionation by diffusion in silicate melts can be simulated by FPMD as demonstrated by two recent computational studies of the diffusive separation of Mg isotopes in MgSiO₃ and Mg₂SiO₄ melts (Liu et al., 2018; Luo et al., 2020). These studies represent significant progress in constraining temperature, pressure, and compositional dependence of β , as well as gaining insights into the underlying atomistic mechanisms. The approach used to simulate and resolve the relatively small differences in the diffusivities of isotopes is called pseudo-isotope method, which has been widely used in molecular dynamics (MD) simulations of isotopes in melts and aqueous solutions (Bourg et al., 2010; Bourg and Sposito, 2007, 2008; Goel et al., 2012; Tsuchiyama et al., 1994; Zeebe, 2011). It should be stressed that Luo et al. (2020) have demonstrated, for major elements in silicate melts, partial substitution of normal-mass isotopes with pseudo-mass ones is necessary to account for the coupled diffusion of isotopes themselves. Coupled diffusion of isotopes may not be a concern for trace elements (e.g. Li) because their isotopes are far away from each other spatially in melts or solutions so that the coupled effects on β may be negligible.

However, due to the high computational cost of FPMD simulations, its typical application to investigate diffusion in silicate melts is restricted to major elements and temperature of >2200 K at the time scale of ~100 picoseconds. It is practically impossible to obtain an accurate estimation of diffusivities of trace elements (e.g. Li) in silicate melts at relatively lower temperatures due to the poor sampling. The advances in machine learning methods have been shown to be useful to model interatomic potentials in the past few years (Bartok et al., 2010; Behler and Parrinello, 2007; Chmiela et al., 2017; Wang et al., 2018; Zhang et al., 2018). Especially, deep potential molecular dynamics (DPMD) simulations (Wang et al., 2018; Zhang et al., 2018), based on the potential energy and interatomic forces generated by a deep neural network trained with *ab initio* data, have been demonstrated to enable us to conduct molecular simulations orders of

magnitude faster than FPMD without sacrificing *ab initio* accuracy (Andrade et al., 2020; Bonati and Parrinello, 2018; Ko et al., 2019; Wang et al., 2018; Xu et al., 2020; Zhang et al., 2018). Thus, DPMD may be a powerful tool to study the diffusion of trace elements and their isotopes in silicate melts and to extend the temperature range explored by typical FPMD simulations.

In this study, we performed DPMD simulations to investigate the temperature and compositional dependence of β for Li isotopes in three silicate melts, albite, hydrous albite, and model basalt, at temperature range 4000 to 1800 K. Albite and model basalt melts can be regarded as close analogs of natural rhyolite (silicic) and basalt melts, respectively. We anticipate that our results and analysis help better constrain the β values and gain microscopic insights for the diffusive behavior of Li isotopes in silicate melts.

2. METHODS

The initial step of performing deep potential molecular dynamics (DPMD) simulations is to obtain train data by conducting first-principles molecular dynamics (FPMD) simulations. FPMD simulations of Li-bearing albite, hydrous albite, and model basalt melts were conducted within local density approximation (Ceperley and Alder, 1980) and projector augmented wave method (Blochl, 1994; Kresse and Joubert, 1999) using Vienna Ab-initio Simulation Package (Kresse and Furthmüller, 1996). We used a plane-wave cutoff energy of 400 eV and Gamma-point Brillouin-zone sampling. A canonical ensemble (*NVT*) with periodic boundary conditions was adopted. The initial supercells of albite and hydrous albite melts contained 8 NaAlSi₃O₈ (104 atoms total), and 8 NaAlSi₃O₈ and 6 H₂O for ~5 wt% water (122 atoms total), respectively. One Na ion was substituted for one Li ion, which corresponds to 0.33 wt% and 0.32 wt% lithium in albite and hydrous albite melts, respectively. The initial supercell of model basalt is the eutectic composition of 36 wt% anorthite and 64 wt% diopside, with the stoichiometry Ca₉Mg₆Al₆Si₁₈O₆₀ (99 atoms total). One Ca and one Mg ion were substituted for one Al and one Li ion, which maintains the charge balance and

corresponds to 0.33 wt% lithium. The simulations of the three silicate melts were performed at 4000, 3000, 2300, and 1800 K at near-zero pressure for ~100 picoseconds (ps). A time step of 1 femtosecond (fs) was used for albite and model basalt melts and of 0.5 femtoseconds for hydrous albite melts. Further details of these simulations can be found in Karki et al. (2018) and Luo et al. (2020).

DeePMD-kit, a deep learning package for interatomic potential energy and force field (Wang et al., 2018; Zhang et al., 2018), was applied to train the potential energy surfaces of the three silicate melts at the four different temperatures, respectively, i.e. in total twelve models were trained. 80% of the corresponding snapshots from the FPMD trajectories were used for training and 20% to test the predictions. Each frame was labeled with energy and forces. We used three hidden layers with 240 nodes per layer. The start learning rate, decay steps, and decay rate were set to 0.001, 2000, and 0.95. Each model was trained for 400000 steps. Once a converged deep potential (DP) model was obtained, we carried out molecular dynamics (MD) using the LAMMPS package (Plimpton, 1995) interfaced with the DeePMD-kit. We adopted a pseudo-isotope approach to simulate the diffusive behavior of Li isotopes with masses $M^* = 2$, 7, 21, 42 g/mol. That is, normal Li ($M^* = 7$) was substituted for Li pseudo-isotopes (e.g. $M^* = 2$) in independent simulations. The time step was set to be the same as that of FPMD simulations. Each simulation ran up to 2 nanoseconds (ns). Configuration was saved every 0.01 ps. For comparison, we adopted the same pseudo-isotope approach and extended the FPMD simulations of albite and model basalt melts at 4000 and 3000 K to 200 ps, provided us an estimation of diffusivities of Li isotopes.

Finite-size effects on diffusion coefficients of Li were shown to be insignificant by simulating 16 NaAlSi₃O₈(208 atoms total) with one Na ion substituted for one Li ion, at 4000 K (Fig. S1). We performed one set of simulations of Li-bearing albite melts within the generalized gradient approximation (GGA) at 4000 K to explore the influence of the choice of exchange-correlation functional on β for Li. It is shown that the β value calculated within GGA is slightly larger (insignificant within uncertainty) than that calculated within the local density approximation (LDA), although the diffusion coefficients of Li pseudo-isotopes are noticeably different (Fig. S2). Note that other systematic effects (e.g. finite size) on diffusion

coefficients can largely be canceled out as well when calculating β by dividing two diffusion coefficients of isotopes using Eq. (1).

The self-diffusion coefficient D_{α} of species α in melts (which represents a Li pseudo-isotope in our case) was calculated using the Einstein relation (Einstein, 1956):

153
$$D_{\alpha} = \lim_{t \to \infty} \frac{\left\langle |\vec{r}(t+t_0) - \vec{r}(t)|^2 \right\rangle_{\alpha}}{6t}, \tag{2}$$

where $\vec{r}(t)$ represents the particle trajectories and $\langle ... \rangle_{\alpha}$ denotes average mean square displacement (MSD) over time and over all atoms of the species α from different time origins t_0 . The infinite time limit in Eq. (2) was approximated by averaging D_{α} for the first picosecond after a clear diffusive regime is attained. Longer time intervals (~5-20 ps) were adopted when the starting time of the diffusive regime cannot be clearly identified. Confidence intervals on D_{α} are reported as ± 2 SE using the blocking method. The value of β and its error in Eq. (1) for Li isotopes can be then derived from the linear fitting in the plot of logD versus logM (Fig. 5).

3. RESULTS

3.1 Validation of DPMD

As shown in Fig. 1, the total radial distribution functions calculated from 2 ns DPMD simulations agree very well with that obtained from 100 ps FPMD simulations for all the three silicate melts, albite, hydrous albite, and model basalt, at temperature from 4000 to 1800 K. Calculated diffusion coefficients of Li isotopes (²Li, ⁷Li, ²¹Li, ⁴²Li) from 2 ns DPMD simulations of the three silicate melts at 4000 and 3000 K also compare well, within their uncertainties, with that estimated from 200 ps FPMD simulations of albite and model basalt melts and 100 ps FPMD simulations of hydrous albite melts (Fig. 2). The root-mean-square error (RMSE) of the energies and forces of our DP models are reported in Table 1.



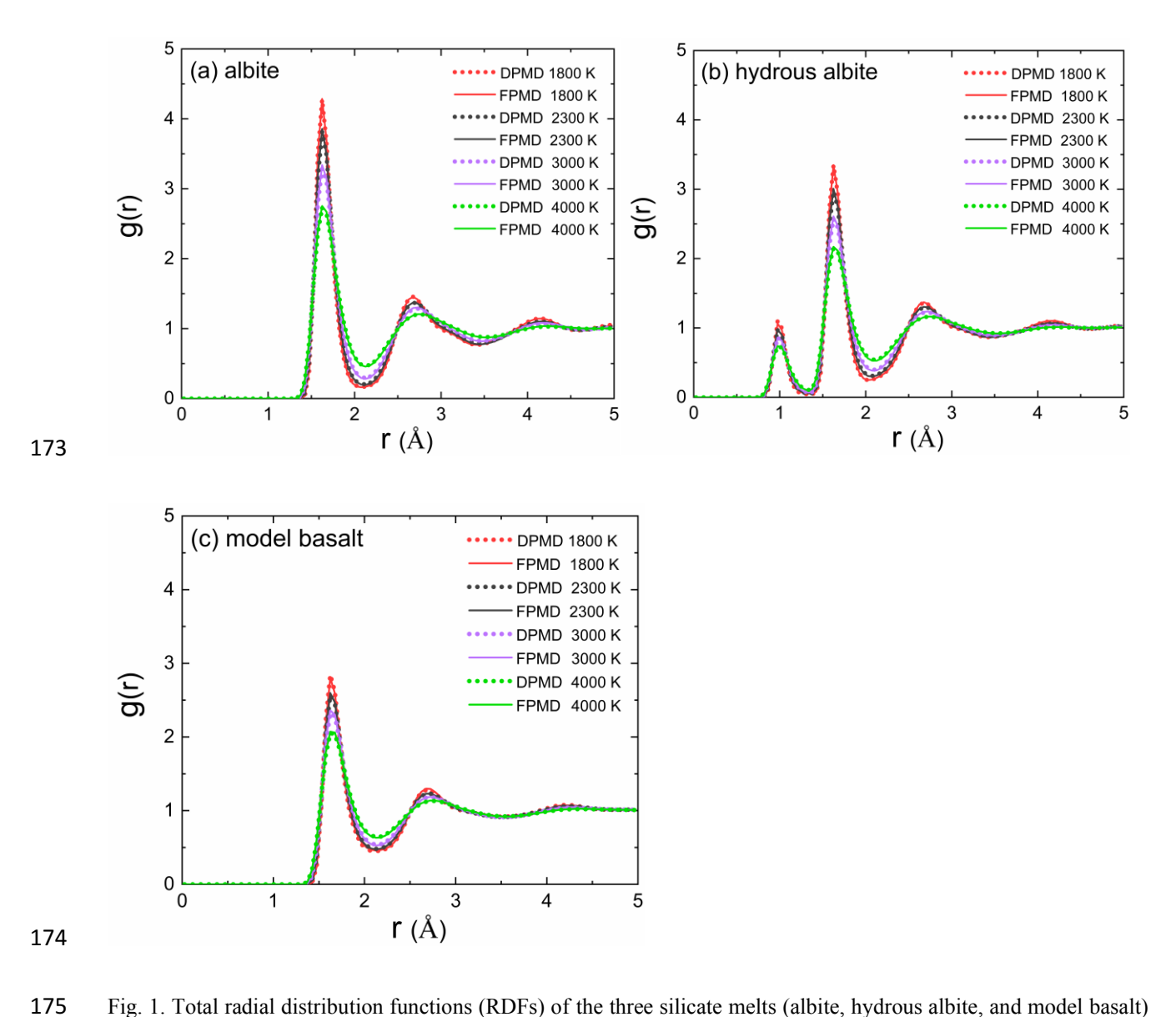
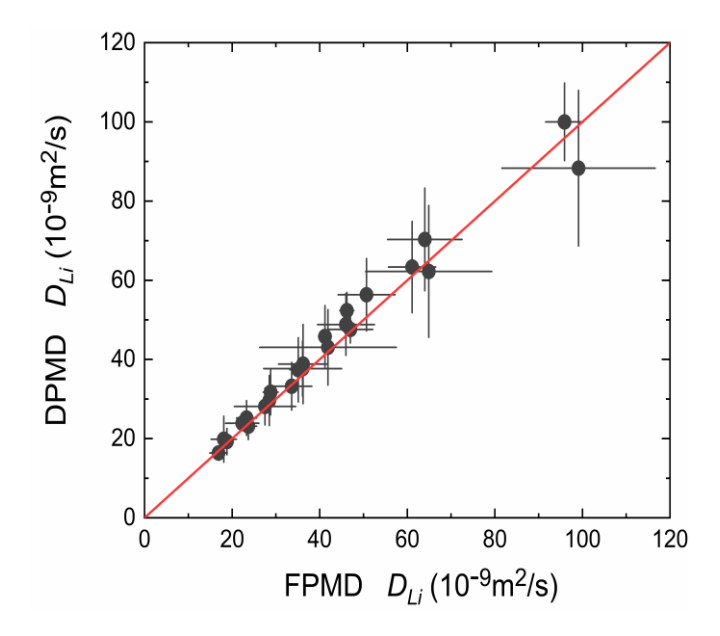


Fig. 1. Total radial distribution functions (RDFs) of the three silicate melts (albite, hydrous albite, and model basalt) at four temperatures (4000, 3000, 2300, and 1800 K) calculated from DPMD and FPMD simulations, respectively.



180

182

183

Table 1

Fig. 2. Diffusion coefficients of Li isotopes (²Li, ⁷Li, ²¹Li, ⁴²Li) in albite, hydrous albite, and model basalt melts at
 4000 and 3000 K calculated from DPMD and FPMD simulations, respectively.

The root-mean-square error of energies and forces of the DP models with training data from FPMD simulations.

System	<i>T</i> (K)	Energy (meV/atom)	Force (meV/Å)
albite	1800	1.38	108
	2300	1.65	121
	3000	2.96	162
	4000	5.05	223
hydrous albite	1800	1.47	136
	2300	1.97	157
	3000	3.27	191
	4000	4.43	232
model basalt	1800	1.55	124
	2300	2.32	135
	3000	3.17	164
	4000	3.13	201

3.2 Temperature and compositional dependence of Li pseudo-isotope diffusivities

We present the calculated diffusivities for Li pseudo-isotopes from 2 ns DPMD simulations of albite, hydrous albite, and model basalt melts at 4000, 3000, 2300, and 1800 K at near-zero pressure in Table 2. Diffusion coefficients of Li pseudo-isotopes correlate negatively with mass and positively with temperature in all the three silicate melts (Fig. 3). Li diffuses much faster in albite melt than in model basalt melt. Water in hydrous albite melt tends to enhance the mobility of all atoms, but its effects are more evident for slow-diffusing Si, O, and Al than fast-diffusing Li and Na. The temperature dependence of diffusivities can be described by the Arrhenius relation:

Table 2

$$D_{\alpha} = D_{0\alpha} exp\left[\frac{-E_{\alpha}}{RT}\right],\tag{3}$$

where α represents Li isotope, R is the universal gas constant, E_{α} is called the activation energy, and the pre-exponential factor $(D_{0\alpha})$ is the value of D_{α} as temperature (T) approaches ∞ . As shown in Table 3, both $D_{0\alpha}$ and E_{α} for the diffusion of Li pseudo-isotopes show a decreasing trend with increasing mass. Based on the fitted linear relation of E_{α} versus logM in Fig. 4, E_{α} for normal mass ⁷Li in albite melt is 66.8 ± 0.3 kJ/mol, much lower the value of 86.0 ± 1.8 kJ/mol in model basalt melt. The presence of \sim 5 wt% water in hydrous albite melt reduces E_{α} to 57.0 ± 3.5 kJ/mol. The fitted $D_{0\alpha}$ and E_{α} for the diffusion of other atomic species are reported in Table 4. E_{α} for Na is comparable to that for Li. E_{α} for Si, O, and Al in model basalt melts are much lower than that in albite melts. The addition of \sim 5 wt% water in hydrous albite melt decreases the E_{α} for Si, O, and Al by \sim 28-35%.

Diffusivities of Li isotopes (with mass M_{α}) and other atoms in albite, hydrous albite, and model basalt melts at different temperatures at near-zero pressure (± 1 GPa). At 1800 K, the diffusivities of O, Al, and Si in albite melts are

not reported because our simulations did not achieve an acceptable convergence of their diffusivities within 2 ns.

albite	T (K)	M_{lpha} (g/mol)	D_{α} (10 ⁻⁹ m ² /s)	D_{Na} (10 ⁻⁹ m ² /s)	$D_O = (10^{-9} \text{m}^2/\text{s})$	D_{Al} (10 ⁻⁹ m ² /s)	D_{Si} (10-9m ² /s)
	4000	2	88.3 ± 19.6	40.3 ± 0.4	9.21 ± 0.18	8.77 ± 0.01	6.73 ± 0.17
	4000	7	62.2 ± 16.6	38.7 ± 1.9	9.22 ± 0.38	8.77 ± 0.22	6.72 ± 0.20
	4000	21	47.6 ± 3.4	38.3 ± 2.7	9.25 ± 0.22	8.64 ± 0.49	6.68 ± 0.29

	4000	42	38.8 ± 10.0	37.8 ± 6.8	9.29 ± 0.04	9.05 ± 0.16	6 6.69 \pm	0.17
	3000	2	43.1 ± 9.5	19.1 ± 0.8	1.06 ± 0.01	1.24 ± 0.02	$0.67 \pm$	0.02
	3000	7	31.7 ± 5.7	19.5 ± 0.8	1.03 ± 0.02	1.32 ± 0.03	$0.65 \pm$	0.01
	3000	21	23.9 ± 1.9	18.9 ± 0.7	1.09 ± 0.03	1.21 ± 0.02	$0.66 \pm$	0.02
	3000	42	19.9 ± 5.8	19.1 ± 1.2	1.08 ± 0.01	1.25 ± 0.10	0 0.69 \pm	0.02
	2300	2	21.0 ± 1.7	9.33 ± 0.91	0.079 ± 0.003	0.087 ± 0.06	0.048 \pm	0.002
	2300	7	15.9 ± 0.7	8.92 ± 0.43	0.073 ± 0.007	0.089 ± 0.00	0.035 ±	0.003
	2300	21	12.5 ± 3.9	9.78 ± 0.78	0.10 ± 0.01	0.12 ± 0.03	$0.055 \pm$	0.002
	2300	42	9.72 ± 0.65	9.27 ± 0.72	0.062 ± 0.002	0.052 ± 0.00	0.034 ±	0.001
	1800	2	6.97 ± 0.66	5.05 ± 0.42				
	1800	7	5.22 ± 0.97	4.88 ± 0.62				
	1800	21	4.05 ± 0.09	5.30 ± 0.34				
	1800	42	3.53 ± 0.06	4.38 ± 0.20				
hydrous albite	T (K)	M_{α} (g/mol)	D_{α} (10 ⁻⁹ m ² /s)	D_{Na} (10 ⁻⁹ m ² /s)	D_H (10 ⁻⁹ m ² /s)	$D_O = (10^{-9} \text{m}^2/\text{s})$	D_{Al} (10 ⁻⁹ m ² /s)	D_{Si} (10 ⁻⁹ m ² /s)
	4000	2	100 ± 9.8	43.0 ± 2.5	60.3 ± 1.0	13.0 ± 0.2	11.7 ± 0.5	9.04 ± 0.55
	4000	7	70.3 ± 13.0	41.3 ± 1.7	61.5 ± 2.3	12.9 ± 0.2	11.4 ± 0.3	8.95 ± 0.30
	4000	21	56.4 ± 9.1	41.0 ± 1.9	60.4 ± 2.9	12.7 ± 0.1	11.3 ± 1.1	8.94 ± 0.34
	4000	42	45.8 ± 7.8	40.8 ± 1.2	59.9 ± 1.5	12.7 ± 0.1	11.4 ± 1.4	8.76 ± 0.11
	3000	2	52.3 ± 4.6	22.1 ± 1.9	19.3 ± 0.5	2.47 ± 0.02	2.54 ± 0.06	1.48 ± 0.03
	3000	7	37.4 ± 8.1	21.6 ± 1.1	19.3 ± 0.3	2.41 ± 0.03	2.56 ± 0.25	1.42 ± 0.02
	3000	21	29.6 ± 6.3	22.7 ± 2.5	18.7 ± 0.2	2.42 ± 0.06	2.43 ± 0.08	1.42 ± 0.09
	3000	42	25.2 ± 4.4	20.9 ± 1.0	19.5 ± 0.7	2.52 ± 0.04	2.80 ± 0.12	1.55 ± 0.01
	2300	2	26.3 ± 2.3	11.6 ± 1.32	5.65 ± 0.08	0.46 ± 0.02	0.45 ± 0.02	0.23 ± 0.01
	2300	7	20.4 ± 1.9	10.9 ± 0.57	5.85 ± 0.33	0.42 ± 0.01	0.46 ± 0.01	0.17 ± 0.01
	2300	21	15.2 ± 1.8	11.6 ± 0.56	6.16 ± 0.40	0.47 ± 0.02	0.45 ± 0.01	0.22 ± 0.01
	2300	42	12.8 ± 3.5	11.3 ± 0.68	5.89 ± 0.41	0.42 ± 0.02	0.44 ± 0.03	0.20 ± 0.00
	1800	2	11.5 ± 0.4	5.11 ± 0.27	1.64 ± 0.03	0.080 ± 0.005	0.047 ± 0.002	0.029 ± 0.001
	1800	7	9.69 ± 1.09	4.99 ± 0.35	1.31 ± 0.02	0.054 ± 0.003	0.049 ± 0.002	0.026 ± 0.000
	1800	21	7.25 ± 3.01	4.87 ± 0.28	1.35 ± 0.05	0.066 ± 0.001	0.049 ± 0.003	0.027 ± 0.002
	1800	42	5.73 ± 0.27	4.44 ± 0.05	1.52 ± 0.05	0.097 ± 0.002	0.039 ± 0.001	0.025 ± 0.001
model basalt	T (K)	M_{lpha} (g/mol)	D_{α} (10 ⁻⁹ m ² /s)	D_{Mg} (10 ⁻⁹ m ² /s)	D_{Ca} (10-9m ² /s)	$D_O (10^{-9} \text{m}^2/\text{s})$	D_{Al} (10-9 m ² /s)	D_{Si} (10 ⁻⁹ m ² /s)
	4000	2	63.3 ± 11.5	18.4 ± 0.9	16.7 ± 1.6	12.3 ± 0.1	11.1 ± 1.1	8.72 ± 0.41
	4000	7	48.8 ± 7.8	17.6 ± 0.6	16.5 ± 0.1	12.1 ± 0.0	10.7 ± 1.0	8.70 ± 0.28
	4000	21	37.7 ± 6.9	18.3 ± 1.3	16.7 ± 0.3	12.1 ± 0.0	11.0 ± 0.4	8.51 ± 0.14
	4000	42	33.2 ± 6.0	18.8 ± 0.6	16.7 ± 0.6	12.1 ± 0.2	10.5 ± 1.2	8.60 ± 0.47
	3000	2	28.1 ± 4.7	7.26 ± 0.53	6.42 ± 0.54	3.20 ± 0.07	3.16 ± 0.15	2.17 ± 0.04
	3000	7	23.1 ± 3.4	6.82 ± 0.35	6.37 ± 0.10	3.13 ± 0.07	3.17 ± 0.12	2.09 ± 0.11
	3000	21	19.2 ± 3.3	6.73 ± 0.98	6.34 ± 0.47	3.17 ± 0.06	3.19 ± 0.06	2.11 ± 0.07
	3000	42	16.4 ± 1.2	6.88 ± 0.06	6.15 ± 0.15	3.10 ± 0.03	3.08 ± 0.09	2.10 ± 0.06
	2300	2	10.1 ± 0.46	2.03 ± 0.23	1.82 ± 0.05	0.77 ± 0.02	0.72 ± 0.02	0.47 ± 0.01
	2300	7	8.34 ± 0.91	2.08 ± 0.11	1.82 ± 0.04	0.75 ± 0.02	0.72 ± 0.02	0.47 ± 0.05
	2300	21	6.91 ± 0.96	2.10 ± 0.33	1.88 ± 0.01	0.77 ± 0.02	0.83 ± 0.02	0.52 ± 0.02
	2300	42	6.38 ± 1.29	2.04 ± 0.07	1.90 ± 0.02	0.75 ± 0.02	0.71 ± 0.06	0.51 ± 0.01

1800	2	2.45 ± 0.38	0.33 ± 0.01	0.29 ± 0.02	0.11 ± 0.00	0.12 ± 0.01	0.069 ± 0.001
1800	7	1.99 ± 0.16	0.39 ± 0.00	0.33 ± 0.02	0.14 ± 0.00	0.15 ± 0.01	0.076 ± 0.003
1800	21	1.84 ± 0.19	0.38 ± 0.02	0.38 ± 0.02	0.14 ± 0.00	0.16 ± 0.01	0.080 ± 0.006
1800	42	1.60 ± 0.04	0.34 ± 0.02	0.33 ± 0.01	0.11 ± 0.01	0.13 ± 0.02	0.070 ± 0.002

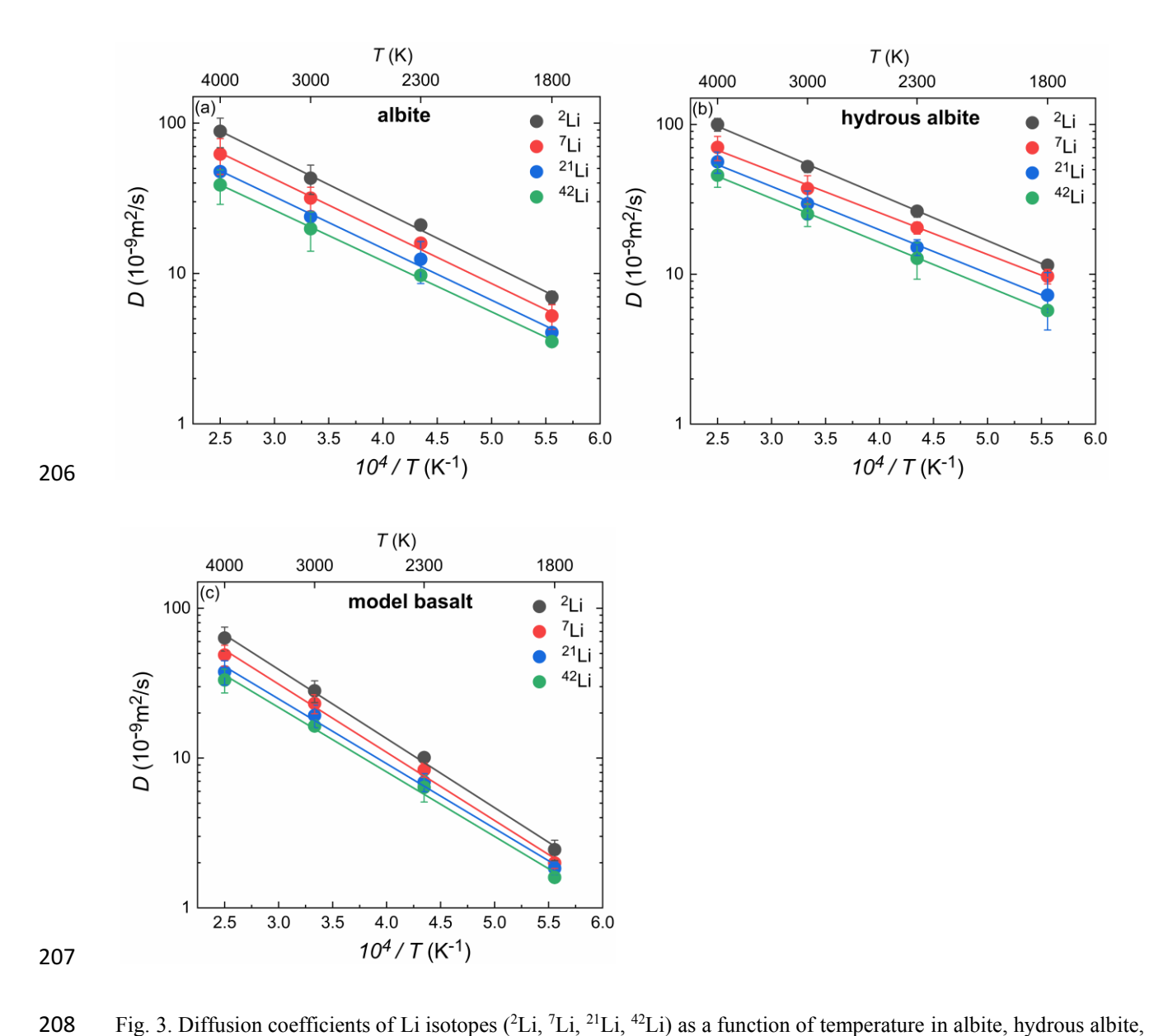


Fig. 3. Diffusion coefficients of Li isotopes (²Li, ⁷Li, ²¹Li, ⁴²Li) as a function of temperature in albite, hydrous albite, and model basalt melts at near-zero pressure.

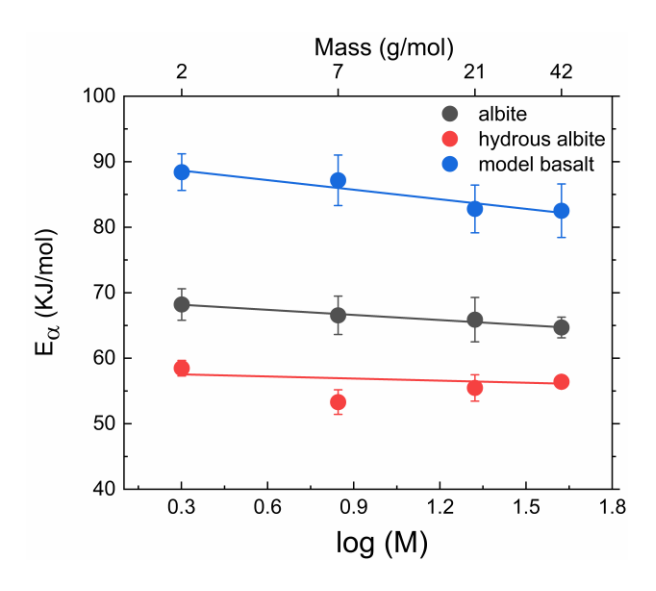


Fig. 4. Activation energies of Li isotopes (²Li, ⁷Li, ²¹Li, ⁴²Li) as a function of isotopic mass in albite, hydrous albite, and model basalt melts at near-zero pressure.

	M_{α}	D_{0lpha}	E_{lpha}
	(g/mol)	$(10^{-9} \text{m}^2/\text{s})$	(kJ/mol)
albite	2	689 ± 82	68.2 ± 2.4
	7	469 ± 68	66.6 ± 2.9
	21	350 ± 58	65.9 ± 3.4
	42	272 ± 21	64.7 ± 1.6
hydrous albite	2	565 ± 33	58.5 ± 1.2
	7	335 ± 31	53.3 ± 1.9
	21	286 ± 28	55.5 ± 2.0
	42	246 ± 8	56.4 ± 0.7
model basalt	2	949 ± 131	88.4 ± 2.8
	7	723 ± 137	87.2 ± 3.9
	21	492 ± 88	82.8 ± 3.6
	42	428 ± 86	82.5 ± 4.1

219 Table 4

Arrhenius fit parameters for the temperature variations of the diffusivities of atomic species (except Li) in albite, hydrous albite, and model basalt melts at near-zero pressure. The influence of the mass of Li pseudo-isotopes on the diffusivities of other atomic species is insignificant (Table 1). The reported value is the average value after removing the outliers.

	atomic	D_{0lpha}	E_{lpha}
	species	$(10^{-9} \text{m}^2/\text{s})$	(kJ/mol)
albite	Na	259 ± 34	63.9 ± 3.2
	Si	6190 ± 380	227 ± 1
	0	5740 ± 150	214 ± 1
	Al	4850 ± 1420	208 ± 7
hydrous albite	Na	231 ± 14	57.9 ± 4.2
	Н	1170 ± 160	101 ± 4
	Si	893 ± 270	157 ± 2
	0	742 ± 230	140 ± 2
	Al	1050 ± 110	150 ± 1
model basalt	Mg	482 ± 100	107 ± 4
	Са	432 ± 78	106 ± 4
	Si	395 ± 46	129 ± 2
	0	482 ± 50	124 ± 2
	Al	370 ± 23	118 ± 1

3.3 Temperature and compositional dependence of β

The linear correlation of the diffusivities of Li isotopes (2 Li, 7 Li, 21 Li, 42 Li) with their isotopic masses in albite, hydrous albite, and model basalt melts at different temperatures (Fig. 5) allows to reliably compute β values for this trace element in silicate melts. It is shown that the calculated β in albite melts decreases from 0.267 at 4000 K to 0.225 at 1800 K. The presence of water appears to slightly weaken the temperature dependence of β , with β decreasing from 0.250 to 0.228 in hydrous albite melt. The calculated β in model basalt melt takes much smaller values, decreasing from 0.215 to 0.132. Assuming a linear correlation of β with I/T (Fig. 6), we can obtain the following relationships at temperature range 4000 to 1800 K under near-zero pressure (±1 GPa).

albite:
$$\beta = (0.300 \pm 0.003) - (0.013 \pm 0.001) \times 10^4 / T$$
. (4)

235 hydrous albite: $\beta = (0.259 \pm 0.012) - (0.005 \pm 0.003) \times 10^4 / T$. (5)

236 model basalt: $\beta = (0.288 \pm 0.016) - (0.031 \pm 0.004) \times 10^4 / T$. (6)

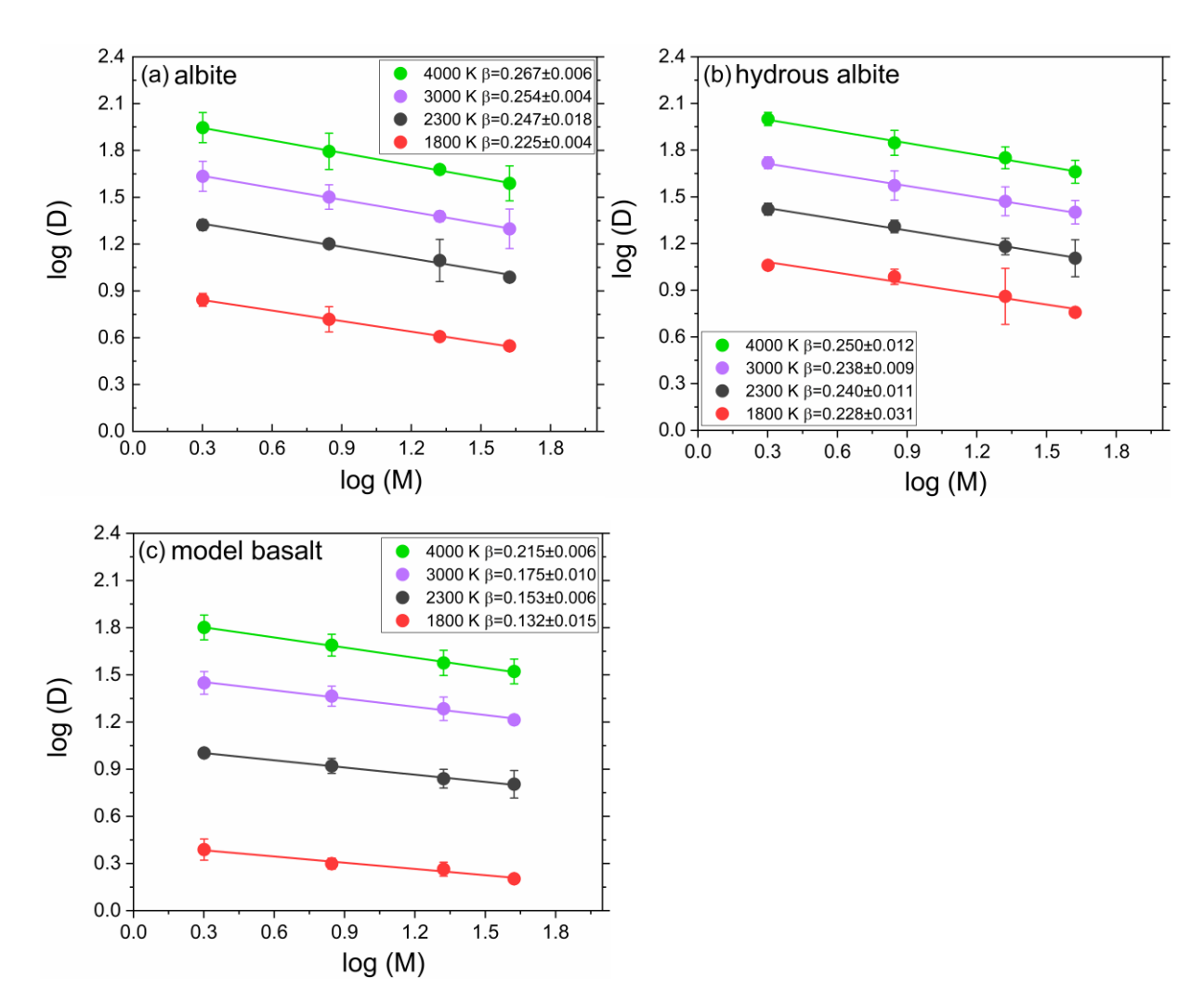


Fig. 5. Log-log plot of diffusivities of Li isotopes (²Li, ⁷Li, ²¹Li, ⁴²Li) in albite, hydrous albite, and model basalt melts at different temperatures at near-zero pressure as a function of isotope mass.

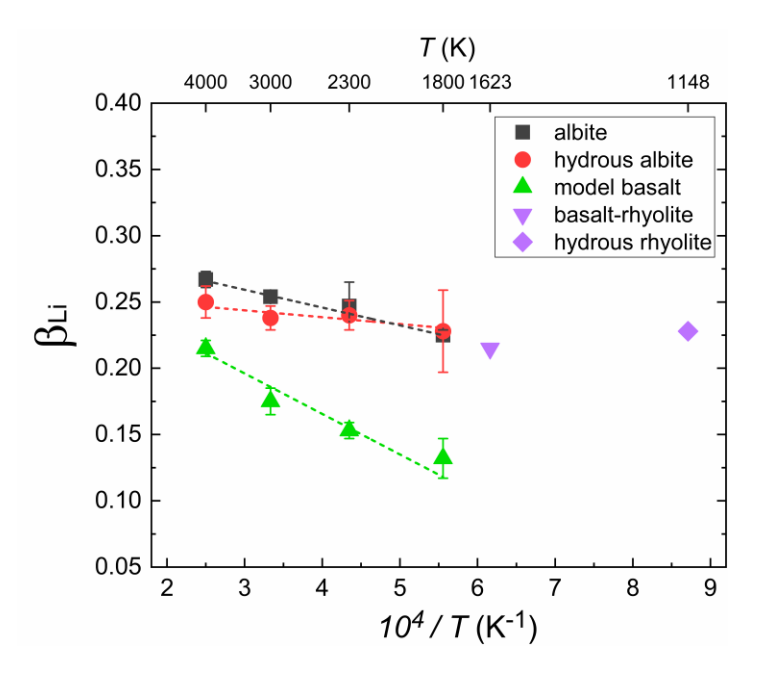


Fig. 6. Correlation of β for Li with temperature in different melts. The β values in albite, hydrous albite, and model basalt melts are obtained from our FPMD simulations. The experimental β values reported in basalt-rhyolite diffusion couple and hydrous rhyolite are from Richter et al. (2003) and Holycross et al. (2018), respectively.

4. DISCUSSION

4.1 Comparison with experimental results

As shown in Fig. 6, previous experiments reported a β of 0.215 in basalt-rhyolite melts at 1623 K (Richter et al., 2003) and a β of 0.228 in hydrous rhyolitic melt at 1063-1148 K (Holycross et al., 2018). Extrapolating the validity of Eq. (4)-(6) from 1800 K to experimental temperatures, our predicted β values are 0.220 \pm 0.003 in albite melt at 1623 K and 0.215 \pm 0.014 in hydrous albite melt at 1148 K, which are in good agreement with experimental results. However, our predicted β in model basalt melt is 0.097 \pm 0.009 at 1623 K, implying that the fitted β value from the diffusion profile of basalt-rhyolite couple is dominated by the β in rhyolitic melt. Our calculations show that β for Li in silicate melts is temperature and composition dependent, and the extent of temperature dependence of β hinges on melt composition. That is, β has a stronger temperature dependence in basaltic melt than that in rhyolitic melt, and the presence of water tends to weaken the temperature dependence of β .

4.2 Mechanism of β

258

259

260

261

262

263

264

265

266

267

268

269

270

271

272

273

274

275

276

277

278

279

280

The mass dependence of diffusion coefficient (Eq. (1)) is an empirical law proposed by Richter et al. (1999). Its applicability has been demonstrated by experiments and molecular dynamics simulations (Watkins et al., 2017), but there is still no diffusion model or theory which postulates the atomic mechanism of determining the magnitude of β in silicate melts. Here several factors, including bond-breaking rate, coupling with melt matrix, and ionic porosity, are examined to explore the mechanism of the temperature and compositional dependence of β for Li.

In silicate melts, Li-O bond-breaking rate (the inverse of average lifetime of a Li-O bond) is a measure of the relative mobility of Li to O and could be correlated with the degree of isotope fractionation by diffusion (Watkins et al., 2011). As shown in Fig. 7, the β for Li indeed decreases with the Li-O bondbreaking rate as the temperature decreases for a particular melt. Among the three simulated melts, the model basalt melts have the slowest bond-breaking rate and also the smallest β value at a given temperature. However, this positive correlation of β with the bond-breaking rate fails to manifest across different temperatures among all three different melts. For example, although the Li-O bond-breaking rate at 3000 K in model basalt melts is larger than that at 2300 K in albite melts, the corresponding β in model basalt melts is much lower than in albite melts. One possible explanation is that the Li-O bond-breaking rate does not necessarily lead to the hop of Li because the hop of coordinated oxygen causes the breaking of the Li-O bond as well, which should result in no diffusive Li isotope fractionation. As shown in Table 2, O diffuses much faster in model basalt melts than in albite melts. Therefore, the difference in the Li-O bond-breaking rate caused only by the hop of Li in the three silicate melts could be larger than that shown in Fig. 7, leading to the mismatch between the Li-O bond-breaking rate and the β value. Another more likely explanation is that diffusive Li isotope fractionation resulted from one hop of Li is composition dependent. That is, one hop of Li in model basalt melts produces smaller Li isotope fractionation than that in the other two melts.

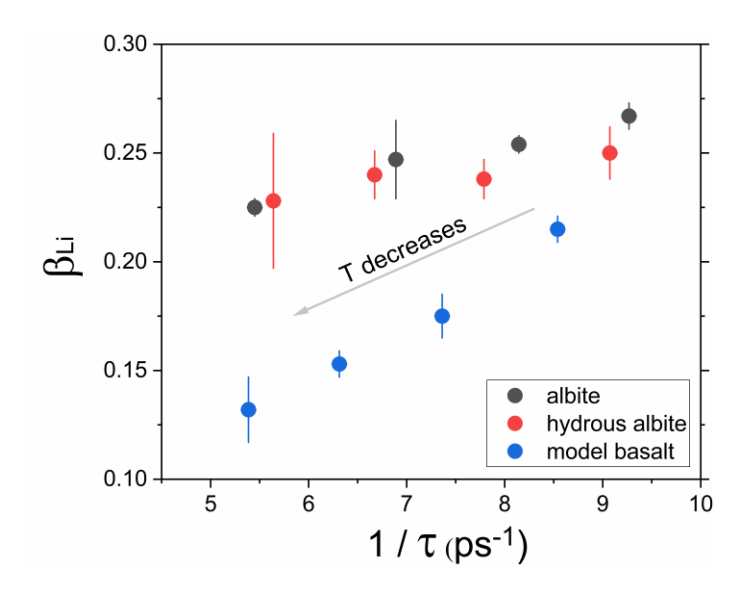


Fig. 7. Correlation of β with ⁷Li-O bond breaking rates (the inverse of average lifetimes of the ⁷Li-O bond) in albite, hydrous albite, and model basalt melts at different temperatures.

Watkins et al. (2011) suggested that there is an empirically positive correlation between solventnormalized diffusivity (D_i/D_{Si}) and β in silicate melts. Based on FPMD simulations of Mg isotopes, Luo et
al. (2020) showed that this positive correlation is applicable only at constant temperatures. Here we examine
if that is the case for the β for Li as well. As shown in Fig. 8a, β for Li shows a positive correlation with D_{Li}/D_{Si} among the three melts at a particular temperature, but a negative correlation with temperature within
a particular melt. There must be other factors impacting the diffusive Li isotope fractionation. D_{Li}/D_{Si} in
model basalt melt is much smaller than that in albite and hydrous albite melts, which is a combined result
of the smallest D_{Li} and the largest D_{Si} among the three melts, a trend becoming more evident with decreasing
temperature. Model basalt melts are less polymerized than the other two melts, leading to the enhancement
of the diffusivity of Si. By contrast, the diffusivity of Li does not obey the generally negative correlation
between diffusivity and the degree of polymerization.

The difference between the diffusive behaviors of Si and Li is consistent with the two classifications of diffusive behaviors of cations, extrinsic and intrinsic diffusivity (Dingwell, 1990). Dingwell. 1990 suggested that ionic porosity, a measure of "free" volume in a structure, may explain the intrinsically

diffusive behavior of Li. The ionic porosity of rhyolitic melt is higher than basaltic melt, making Li diffuse faster in the former. Ionic porosity is defined as $IP = 1 - V_{ions}/V_0$, where V_{ions} is the volume occupied by all ions and V_0 is the volume of the whole structure. To explore the correlation between ionic porosity and diffusive Li isotope fractionation, we calculated the ionic porosities of the three melts. The ionic radiuses of individual anions and cations chosen from Shannon and Prewitt (1969) are the same as those used in previous studies (Carroll and Stolper, 1993; Nuccio and Paonita, 2000), and the volumes of the melt structures are shown in Table S1. We found that the β for Li correlates positively with ionic porosity for any given type of melt constrained here, but β with a higher ionic porosity in model basalts at 4000 K is smaller than that with a lower ionic porosity in albite and hydrous albite melts below 3000 K, which defies the positive correlation (Fig. 8b). The most likely explanation is that the coupled effect between Li diffusion and the mobility of the silicate melt network is stronger in model basalts (Fig. 8a). Therefore, it appears that both the ionic porosity and the coupled relationship between Li diffusion and the mobility of silicate melt network exert an influence on the magnitude of β , which also explains why β with a larger D_{Li}/D_{Si} in model basalt melts at 2300 K is smaller than that with a smaller D_{Li}/D_{Si} in albite and hydrous albite melts at 4000 K in considering the smaller ionic porosity in model basalt melts. For now, it is not possible to resolve the relative contribution of the two effects to the β value. In principle, the two effects on β are consistent with the variation of diffusive behavior of Li as the intrinsic diffusivity curve approaches the extrinsic regime as temperature increases (Dingwell, 2006), and intrinsic diffusivity and extrinsic diffusivity are characterized by ionic porosity and the relationship between cationic diffusion and matrix mobility, respectively.

298

299

300

301

302

303

304

305

306

307

308

309

310

311

312

313

314

315

316

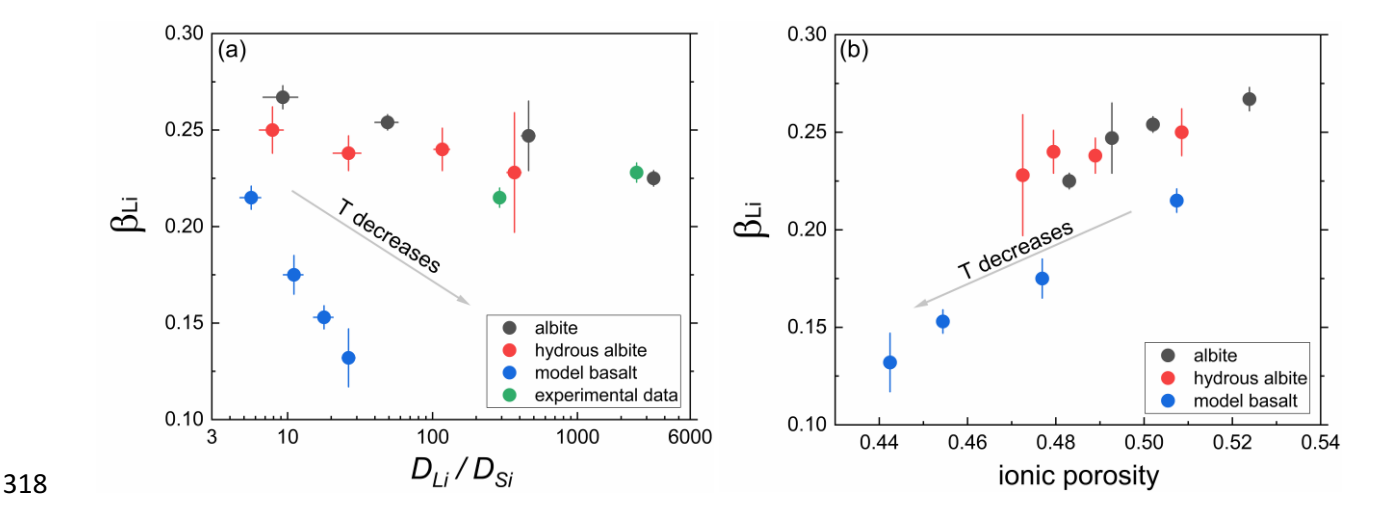


Fig. 8. Relationships of β with D_{Li}/D_{Si} and ionic porosity in albite, hydrous albite, and model basalt melts at different temperatures. D_{Si} in albite melts at 1800 K is obtained from our calculated Arrhenius relation. Experimental data are from Richter et al. (2003) and Holycross et al. (2018).

4.3 Geological implications

Diffusive Li isotope fractionation has been widely used to explain observed Li isotope variations in natural high-temperature materials (Penniston-Dorland et al., 2017; Tomascak et al., 2016). Li isotope fractionation by diffusion in silicate melts matters in the geological processes including magma degassing (Cabato et al., 2013; Ellis et al., 2018; Neukampf et al., 2019; Vlastelic et al., 2011) and mineral-melt interactions (Jeffcoate et al., 2007; Lundstrom et al., 2005; Parkinson et al., 2007). Diffusive Li isotope fractionation might occur during bubble growth (Watson, 2017). β for Li must be firstly determined to estimate the loss of Li and to infer the original Li isotope composition of melts and their mantle sources. The diffusive loss of Li isotopes from melt inclusions or embayments also may aid to investigate magma-ascent rates (Myers et al., 2019). During mineral-melt interactions, diffusive fractionation during rapid crystal growth under certain conditions might lead to an isotopic signature in crystals, which can be altered by diffusive mineral-melt re-equilibration during slow cooling and by diffusive ingression of a grain boundary melt with distinct Li isotope composition during metamorphic processes (Jeffcoate et al., 2007). As our simulated results suggest, we must consider the extent of temperature and compositional dependence

of diffusive Li isotope fractionation when we interpret Li isotope composition of natural, high-temperature materials and to extract information altered or recorded by diffusive separation of Li isotopes.

It is worth stressing that the DPMD method we used in this study and its related methods (e.g. DPGEN) have achieved some remarkable success in physics, chemistry, and material science areas in the past two years (Andrade et al., 2020; Bonati and Parrinello, 2018; Ko et al., 2019; Xu et al., 2020; Zhang et al., 2019), but they have barely been used in Earth science. These new methods based on deep neural network have the potential to revolutionize diffusion simulation of elements and isotopes in Earth materials.

5. CONCLUSIONS

We performed a series of DPMD simulations to explore the temperature and compositional dependence of β for Li in silicate melts. Our results showed that DPMD simulations combined with the pseudo-isotope method is reliable to obtain diffusive isotope fractionation for trace elements (e.g. Li) in silicate melts. Calculated β for Li is temperature and composition dependent, and the extent of temperature dependence of β hinges on melt composition. That is, β has a stronger temperature dependence in basaltic melt than that in rhyolitic melt, and the presence of water tends to weaken the temperature dependence of β . The combined effect of ionic porosity and the coupled relationship between Li diffusion and the mobility of the silicate melt network may explain the temperature and compositional dependence of β . Our results suggest that a self-diffusion or tracer diffusion experiment of Li isotopes in a basaltic or CaO-MgO-Al₂O₃-SiO₂ (CMAS) melt should be designed to further test the compositional dependence of β .

ACKNOWLEDGMENTS

The research is supported by the Strategic Priority Research Program (B) of Chinese Academy of Sciences (XDB18010104) and National Science Foundation (EAR 1764140). High-performance computing resources were provided by Louisiana State University.

360

361

367

368

376

377

378

379

380

381

382

383

384

385

386

387

388

389

390

391

392

393

394

395

357

358

359

REFERENCES

- 362 Andrade, M.F.C., Ko, H.Y., Zhang, L.F., Car, R., Selloni, A., 2020. Free energy of proton transfer at the 363 water-TiO2 interface from ab initio deep potential molecular dynamics. Chemical Science 11, 364 2335-2341.
- 365 Bartok, A.P., Payne, M.C., Kondor, R., Csanyi, G., 2010. Gaussian Approximation Potentials: The Accuracy 366 of Quantum Mechanics, without the Electrons. Phys Rev Lett 104.
 - Behler, J., Parrinello, M., 2007. Generalized neural-network representation of high-dimensional potential-energy surfaces. Phys Rev Lett 98.
- 369 Bigeleisen, J., Mayer, M.G., 1947. Calculation of Equilibrium Constants for Isotopic Exchange Reactions. J 370 Chem Phys 15, 261-267.
- 371 Blochl, P.E., 1994. Projector Augmented-Wave Method. Phys Rev B 50, 17953-17979.
- 372 Bonati, L., Parrinello, M., 2018. Silicon Liquid Structure and Crystal Nucleation from Ab Initio Deep 373 Metadynamics. Phys Rev Lett 121.
- 374 Bourg, I.C., Richter, F.M., Christensen, J.N., Sposito, G., 2010. Isotopic mass dependence of metal cation 375 diffusion coefficients in liquid water. Geochim Cosmochim Ac 74, 2249-2256.
 - Bourg, I.C., Sposito, G., 2007. Molecular dynamics simulations of kinetic isotope fractionation during the diffusion of ionic species in liquid water. Geochim Cosmochim Ac 71, 5583-5589.
 - Bourg, I.C., Sposito, G., 2008. Isotopic fractionation of noble gases by diffusion in liquid water: Molecular dynamics simulations and hydrologic applications. Geochim Cosmochim Ac 72, 2237-2247.
 - Cabato, J., Altherr, R., Ludwig, T., Meyer, H.P., 2013. Li, Be, B concentrations and delta Li-7 values in plagioclase phenocrysts of dacites from Nea Kameni (Santorini, Greece). Contrib Mineral Petr 165, 1135-1154.
 - Carroll, M.R., Stolper, E.M., 1993. NOBLE-GAS SOLUBILITIES IN SILICATE MELTS AND GLASSES NEW EXPERIMENTAL RESULTS FOR ARGON AND THE RELATIONSHIP BETWEEN SOLUBILITY AND IONIC POROSITY. Geochim Cosmochim Ac 57, 5039-5051.
 - Ceperley, D.M., Alder, B.J., 1980. Ground-State of the Electron-Gas by a Stochastic Method. Phys Rev Lett 45, 566-569.
 - Charlier, B.L.A., Morgan, D.J., Wilson, C.J.N., Wooden, J.L., Allan, A.S.R., Baker, J.A., 2012. Lithium concentration gradients in feldspar and quartz record the final minutes of magma ascent in an explosive supereruption. Earth Planet Sc Lett 319, 218-227.
 - Chmiela, S., Tkatchenko, A., Sauceda, H.E., Poltavsky, I., Schutt, K.T., Muller, K.R., 2017. Machine learning of accurate energy-conserving molecular force fields. Science Advances 3.
 - Coogan, L.A., Kasemann, S.A., Chakraborty, S., 2005. Rates of hydrothermal cooling of new oceanic upper crust derived from lithium-geospeedometry. Earth Planet Sc Lett 240, 415-424.
- Costa, F., Shea, T., Ubide, T., 2020. Diffusion chronometry and the timescales of magmatic processes. 396 Nature Reviews Earth & Environment 1, 201-214.
- 397 Dingwell, D.B., 1990. EFFECTS OF STRUCTURAL RELAXATION ON CATIONIC TRACER DIFFUSION IN 398 SILICATE MELTS. Chem Geol 82, 209-216.

- Dingwell, D.B., 2006. Transport properties of magmas: Diffusion and rheology. Elements 2, 281-286.
- Dohmen, R., Kasemann, S.A., Coogan, L., Chakraborty, S., 2010. Diffusion of Li in olivine. Part I:
- Experimental observations and a multi species diffusion model. Geochim Cosmochim Ac 74, 274-292.
- Einstein, A., 1956. Investigation on the Theory of the Brownian Movement. Courier Corporation.

407

410

411

412

413

414

415

416

417

418

423

424

427

428

429

430

431

- Ellis, B.S., Szymanowski, D., Magna, T., Neukampf, J., Dohmen, R., Bachmann, O., Ulmer, P., Guillong, M., 2018. Post-eruptive mobility of lithium in volcanic rocks. Nat Commun 9.
 - Ghosh, D.B., Karki, B.B., 2011. Diffusion and viscosity of Mg2SiO4 liquid at high pressure from first-principles simulations. Geochim Cosmochim Ac 75, 4591-4600.
- 408 Ghosh, D.B., Karki, B.B., 2017. Transport properties of carbonated silicate melt at high pressure. Science 409 Advances 3.
 - Goel, G., Zhang, L.Q., Lacks, D.J., Van Orman, J.A., 2012. Isotope fractionation by diffusion in silicate melts: Insights from molecular dynamics simulations. Geochim Cosmochim Ac 93, 205-213.
 - Holycross, M.E., Watson, E.B., Richter, F.M., Villeneuve, J., 2018. Diffusive fractionation of Li isotopes in wet, highly silicic melts. Geochem Perspect Let 6, 39-42.
 - Jeffcoate, A.B., Elliott, T., Kasemann, S.A., Ionov, D., Cooper, K., Brooker, R., 2007. Li isotope fractionation in peridotites and mafic melts. Geochim Cosmochim Ac 71, 202-218.
 - Karki, B.B., 2010. First-Principles Molecular Dynamics Simulations of Silicate Melts: Structural and Dynamical Properties. Theoretical and Computational Methods in Mineral Physics: Geophysical Applications 71, 355-389.
- Karki, B.B., Ghosh, D.B., Bajgain, S.K., 2018. Chapter 16 Simulation of Silicate Melts Under Pressure, in: Kono, Y., Sanloup, C. (Eds.), Magmas Under Pressure. Elsevier, pp. 419-453.
- Ko, H.Y., Zhang, L.F., Santra, B., Wang, H., E, W.N., DiStasio, R.A., Car, R., 2019. Isotope effects in liquid water via deep potential molecular dynamics. Molecular Physics 117, 3269-3281.
 - Kresse, G., Furthmuller, J., 1996. Efficiency of ab-initio total energy calculations for metals and semiconductors using a plane-wave basis set. Comp Mater Sci 6, 15-50.
- Kresse, G., Joubert, D., 1999. From ultrasoft pseudopotentials to the projector augmented-wave method. Phys Rev B 59, 1758-1775.
 - Liu, X.H., Qi, Y.H., Zheng, D.Y., Zhou, C., He, L.X., Huang, F., 2018. Diffusion coefficients of Mg isotopes in MgSiO3 and Mg2SiO4 melts calculated by first-principles molecular dynamics simulations. Geochim Cosmochim Ac 223, 364-376.
 - Lundstrom, C.C., Chaussidon, M., Hsui, A.T., Kelemen, P., Zimmerman, M., 2005. Observations of Li isotopic variations in the Trinity Ophiolite: Evidence for isotopic fractionation by diffusion during mantle melting. Geochim Cosmochim Ac 69, 735-751.
- Luo, H., Karki, B.B., Ghosh, D.B., Bao, H., 2020. First-principles computation of diffusional Mg isotope fractionation in silicate melts. Geochimica et Cosmochimica Acta (2020).
- Marschall., H.R., Tang., M., 2020. High-Temperature Processes: Is it Time for Lithium Isotopes? Elements 16.
- Myers, M.L., Wallace, P.J., Wilson, C.J.N., 2019. Inferring magma ascent timescales and reconstructing conduit processes in explosive rhyolitic eruptions using diffusive losses of hydrogen from melt inclusions. Journal of Volcanology and Geothermal Research 369, 95-112.
- Neukampf, J., Ellis, B.S., Magna, T., Laurent, O., Bachmann, O., 2019. Partitioning and isotopic
 fractionation of lithium in mineral phases of hot, dry rhyolites: The case of the Mesa Falls Tuff,
 Yellowstone. Chem Geol 506, 175-186.
- Nuccio, P.M., Paonita, A., 2000. Investigation of the noble gas solubility in H2O-CO2 bearing silicate liquids at moderate pressure II: the extended ionic porosity (EIP) model. Earth Planet Sc Lett 183, 499-512.

- Parkinson, I.J., Hammond, S.J., James, R.H., Rogers, N.W., 2007. High-temperature lithium isotope fractionation: Insights from lithium isotope diffusion in magmatic systems. Earth Planet Sc Lett 257, 609-621.
- Penniston-Dorland, S., Liu, X.M., Rudnick, R.L., 2017. Lithium Isotope Geochemistry, in: Teng, F.Z.,
 Watkins, J., Dauphas, N. (Eds.), Non-Traditional Stable Isotopes. Mineralogical Soc Amer &
 Geochemical Soc, Chantilly, pp. 165-217.

455

456

457

458

459

460

461

462 463

464

465

466

467

468

469

470

471

472

473

474

475

476

477

478

479

480

481

482

483

484

- 452 Plimpton, S., 1995. FAST PARALLEL ALGORITHMS FOR SHORT-RANGE MOLECULAR-DYNAMICS. Journal of Computational Physics 117, 1-19.
 - Richter, F., Chaussidon, M., Watson, E.B., Mendybaev, R., Homolova, V., 2017. Lithium isotope fractionation by diffusion in minerals Part 2: Olivine. Geochim Cosmochim Ac 219, 124-142.
 - Richter, F., Watson, B., Chaussidon, M., Mendybaev, R., Ruscitto, D., 2014. Lithium isotope fractionation by diffusion in minerals. Part 1: Pyroxenes. Geochim Cosmochim Ac 126, 352-370.
 - Richter, F.M., Davis, A.M., DePaolo, D.J., Watson, E.B., 2003. Isotope fractionation by chemical diffusion between molten basalt and rhyolite. Geochim Cosmochim Ac 67, 3905-3923.
 - Richter, F.M., Liang, Y., Davis, A.M., 1999. Isotope fractionation by diffusion in molten oxides. Geochim Cosmochim Ac 63, 2853-2861.
 - Shannon, R.D., Prewitt, C.T., 1969. EFFECTIVE IONIC RADII IN OXIDES AND FLUORIDES. Acta Crystallographica Section B-Structural Crystallography and Crystal Chemistry B 25, 925-&.
 - Tomascak, P.B., Magna, T., Dohmen, R., 2016. Advances in Lithium Isotopes Geochemistry. Springer-Verlag, Berlin.
 - Tomascak, P.B., Tera, F., Helz, R.T., Walker, R.J., 1999. The absence of lithium isotope fractionation during basalt differentiation: New measurements by multicollector sector ICP-MS. Geochim Cosmochim Ac 63, 907-910.
 - Tsuchiyama, A., Kawamura, K., Nakao, T., Uyeda, C., 1994. Isotopic effects on diffusion in MgO melts simulated by the molecular-dynamic (MD) method and implications for isotopic mass fractionation in magmatic systems. Geochim Cosmochim Ac 58, 3013-3021.
 - Urey, H.C., 1947. The Thermodynamic Properties of Isotopic Substances. J Chem Soc, 562-581.
 - Vlastelic, I., Staudacher, T., Bachelery, P., Telouk, P., Neuville, D., Benbakkar, M., 2011. Lithium isotope fractionation during magma degassing: Constraints from silicic differentiates and natural gas condensates from Piton de la Fournaise volcano (Reunion Island). Chem Geol 284, 26-34.
 - Wang, H., Zhang, L.F., Han, J.Q., E, W.N., 2018. DeePMD-kit: A deep learning package for many-body potential energy representation and molecular dynamics. Computer Physics Communications 228, 178-184.
 - Watkins, J.M., DePaolo, D.J., Ryerson, F.J., Peterson, B.T., 2011. Influence of liquid structure on diffusive isotope separation in molten silicates and aqueous solutions. Geochim Cosmochim Ac 75, 3103-3118.
 - Watkins, J.M., DePaolo, D.J., Watson, E.B., 2017. Kinetic Fractionation of Non-Traditional Stable Isotopes by Diffusion and Crystal Growth Reactions. Non-Traditional Stable Isotopes 82, 85-125.
 - Watson, E.B., 2017. Diffusive fractionation of volatiles and their isotopes during bubble growth in magmas. Contrib Mineral Petr 172.
- 486 Xu, N., Shi, Y., He, Y., Shao, Q., 2020. A Deep-Learning Potential for Crystalline and Amorphous Li-Si 487 Alloys. Journal of Physical Chemistry C 124, 16278-16288.
- Zeebe, R.E., 2011. On the molecular diffusion coefficients of dissolved CO2, HCO3-, and CO32- and their dependence on isotopic mass. Geochim Cosmochim Ac 75, 2483-2498.
- Zhang, L.F., Han, J.Q., Wang, H., Car, R., Weinan, E., 2018. Deep Potential Molecular Dynamics: A
 Scalable Model with the Accuracy of Quantum Mechanics. Phys Rev Lett 120.
- Zhang, L.F., Lin, D.Y., Wang, H., Car, R., E, W.N., 2019. Active learning of uniformly accurate interatomic potentials for materials simulation. Physical Review Materials 3.